Phase Diagram and High-Temperature Superconductivity of Selenium Hydrides at High Pressures

Shoutao Zhang[1], Yanchao Wang[1], Hanyu Liu[1], Guochun Yang[2,*], Lijun Zhang[3,*] and Yanming Ma[1,*]

[1]*State Key Laboratory of Superhard Materials, Jilin University, Changchun 130012, China.*

[2]*Faculty of Chemistry, Northeast Normal University, Changchun 130024, China.*

[3]*College of Materials Science and Engineering, Jilin University, Changchun 130012, China*

[*]Address correspondence to: yanggc468@nenu.edu.cn, lijun_zhang@jlu.edu.cn or mym@calypso.cn

ABSTRACT: Recent discovery of high-temperature superconductivity (T_c = 190 K) in sulfur hydrides at megabar pressures breaks the traditional belief on the T_c limit of 40 K for conventional superconductors, and open up the doors in searching new high-temperature superconductors in compounds made up of light elements. Selenium is a sister and isoelectronic element of sulfur, with a larger core and a weaker electronegativity. Whether selenium hydrides share similar high-temperature superconductivity remain elusive, but it is a subject of considerable interest. First-principles swarm structure predictions are performed in an effort to seek for energetically stable and metallic selenium hydrides at high pressures. We find the stable phase diagram of selenium hydrides is different from its sulfur analogy. Three stable and metallic species with stoichiometries of HSe_2, HSe and H_3Se are identified above ~120 GPa and they all exhibit superconductive behaviors, of which the hydrogen-rich HSe and H_3Se phases show high T_c in the range of 40-106 K. Our simulations established the high-temperature superconductive nature of selenium hydrides and provided useful route for experimental verification.

PACS numbers:

Since Onnes discovered superconductivity of mercury in 1911,[1] intensive research activities were stimulated to search for new superconductors with high critical temperatures (T_c). With this thrust, unconventional superconductors such as cuprates[2-4] and Fe-pnictides,[5-7] in which superconducting mechanism cannot be described by Bardeen-Cooper-Schrieffer (BCS) theory[8] have attracted major attention since they often exhibit high T_c values, reaching as high as 164 K at high pressures. [9] In spite of extensive research for several decades, the superconducting mechanism in these unconventional superconductors is still controversial, preventing them from being an optimal design platform toward a higher T_c.

On the side of conventional superconductors, the situation is rather disappointing since they all have low T_c values. The best-known conventional superconductor of MgB_2 has the T_c of 39 K.[10] As such, there is a traditional belief on the T_c limit of 40 K for conventional superconductors in the field.

BCS theory gives a clear count on superconducting mechanism of conventional superconductors, making the design of high T_c superconductors possible. According to BCS theory, a necessary condition for a high-T_c superconductor is that the metallic compounds shall have strong electron-phonon coupling and large electron density of states at the Fermi level. Hydrogen is the lightest element, and therefore naturally give rises to high phonon frequencies, and thus high electron-phonon coupling. Ashcroft firstly proposed that solid hydrogen once being metallic under pressure has the potential to be a high-temperature superconductor.[11] Later on, the idea on metallic superconducting hydrogen was extended into hydrogen-rich compounds,[12] where metallization pressure can be significantly lowered than that in pure hydrogen. A number of hydrogen-rich compounds were subsequently predicted to be good superconductors with estimated T_c reaching remarkably high values (*e.g.* 64 K for GeH_4 at 220 GPa,[13] 107 K for $SiH_4(H_2)_2$ at 250 GPa,[14] 235 K for CaH_6 at 150 GPa,[15] and 204 K for $(H_2S)_2H_2$ at 200 GPa[16]). Experimental syntheses of these potential high-temperature superconductors are exciting, but challenging.

Sulfur dihydride (H_2S) is not considered as the candidate for superconducting hydrides since it was proposed to dissociation into elemental sulfur and hydrogen before the metallization.[17,18] Only recently, first-principles swarm structure searches on high-pressure structures of H_2S was conducted and H_2S was excluded from the elemental dissociation, making the prediction of a high-temperature superconductor with a T_c ~ 80 K at 160 GPa possible.[19] Shortly after this report, breakthrough electrical measurement observed high-temperature superconductivity in compressed H_2S with an unprecedentedly high T_c of ~190 K at 180 GPa.[20] The T_c decrease with magnetic field, and the strong isotope shift of T_c suggest that H_2S is a conventional superconductor. There exist two observed superconducting states: the sample prepared at low temperature of 100-150 K has a maximal T_c of 150 K at 200 GPa, while the 190 K superconductivity is from the sample prepared at high temperature of 220-300 K, which likely associates with the dissociation of H_2S into H_3S.[20-22] This discovery has stimulated significant interest in studying the underlying superconducting mechanism[22-25] and searching for new high-T_c superconductors in other dense hydride systems.

Selenium is a sister and isoelectronic element of sulfur with a larger atomic radius and a weaker electronegativity. By witness of high-T_c superconductivity of sulfur hydride (*i.e.* H-S system), a natural and exciting thought is to examine whether selenium hydrides (H-Se system) are also high-temperature superconductors at high pressures. To our best knowledge, there is less report on solid phases of H-Se system, except for the existence of three temperature-dependent phases at ambient pressure.[26]

For this purpose, we extensively explored the high-pressure phase stability of various selenium hydrides via the first-principles swarm structure searching study. We found the phase diagram of H-Se system at high pressures is distinct from that of H-S system. Three stable and metallic species with stoichiometries of HSe_2, HSe and H_3Se were identified at megabar pressures, which all exhibit superconductive behaviors. The latter two H-rich phases show high T_c values up to 106 K. Our simulations provide a useful roadmap for discovering high-temperature superconductors in selenium hydrides.

The energetic stability of H-Se system is investigated by globally minimizing the potential energy surface at varied stoichiometries via an in-house developed swarm-intelligence based CALYPSO method[27, 28] in combination with *ab initio* density functional theory (DFT) total-energy calculations. Its validity in rapidly finding the stable ground-state structures has been demonstrated by its applications in various material systems ranging from elements to binary and ternary compounds.[27, 29-31] The energetic calculations are performed using the plane-wave pseudopotential method within the generalized gradient approximation through the Perdew–Burke–Ernzerhof (PBE) exchange-correlation functional[32], as implemented in the VASP code.[33] The electron-ion interaction was described by the projected-augmented-wave potentials with $1s^1$ and $4s^24p^4$ as valence electrons for H and Se, respectively. During the structure search, an economy set of parameters are used to calculate the relative energetics of sampled structures, following which the cutoff energy of 600 eV for the expansion of wave-function and Monkhorst−Pack *k*-point sampling with grid spacing of $2\pi \times 0.03$ Å^{-1} were chosen to ensure the enthalpy converged to better than 1 meV/atom. The validity of pseudopotentials used at high pressures is carefully examined with the full-potential linearized augmented plane-wave method through the WIEN2k package.[34] The phonon spectrum for evaluating the lattice dynamic stability and electron-phonon coupling for superconducting properties of stable phases are performed within the framework of the linear-response theory via Quantum-ESPRESSO package.[35]

The variable-composition crystal structure predictions are performed at a variety of stoichiometries containing up to 4 formula units (f.u.) per simulation cell at 0, 100, 200 and 300 GPa. At 0 GPa, the only stable stoichiometry with respect to the elemental decomposition is H_2Se, consistent with experiment.[26] It is in the $P3_12_1$ symmetry, where the arrangement of Se atoms is nearly the same as that in the Se-I phase [36] and H atoms are accommodated on the line of two adjacent Se to form covalent H-Se bond and hydrogen bond simultaneously. However, with increasing pressure this phase becomes dramatically unstable (see Supplemental Fig. S1). The structure search results at high pressures are summarized in the convex hulls with respect to solid H_2 and Se as the binary variables in Fig. 1. As seen, at the lower pressure of 100 GPa, all the stoichiometries are energetically unstable against the elemental decomposition. With increasing pressure to 200 GPa, while most of phases still lie above the decomposition line,

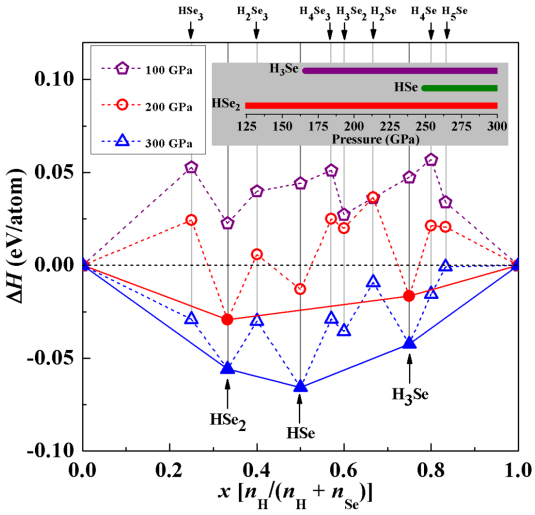

Figure 1. Calculated formation enthalpies (ΔH in eV/atom) of various selenium hydrides at different stoichiometries with respect to the decomposition into solid H_2 and Se at 100 (violet), 200 (red) and 300 (blue) GPa, respectively. At each stoichiometry, only ΔH of the lowest-energy structure is shown. The phase IV ($C2/m$) and phase VI (Im-3m) of Se,[37] the $P6_3m$ and $C2/c$ structure of solid H_2[38] are used at corresponding stable pressure region for calculating decomposition enthalpy. The inset plot shows the stable pressure range of each stable stoichiometry, which is evaluated with respect to decomposing into two adjacent stable stoichiometries on the hull.

three stoichiometries (HSe_2, HSe and H_3Se) show strong trends of being stabilized and move downward below the line. This makes HSe_2 and H_3Se become stable stoichiometries on the hull against any way of decomposition. At the highest pressure of 300 GPa studied, all the three stoichiometries (HSe_2, HSe and H_3Se) are clearly stabilized on the hull, and HSe emerges as the most stable phase over other species.

The Se-rich HSe_2 stoichiometry is the most stable specie at 200 GPa. Its lowest-enthalpy structure (Fig. 2a) has a $C2/m$ symmetry, in which the sublattice of Se atoms is isostructural to the Se-IV phase[37] and H atoms passivate alternatively from both sides of the infinite zigzag Se chain along the perpendicular direction. Its stable pressure range is above 124 GPa (as in the inset of Fig. 1). For HSe, a highly symmetric PbO-type structure (space group $P4/nmm$, Fig. 2b) becomes energetically stable above 249 GPa. This structure, which is isostructural to superconducting layers in Fe-pnicitdes[5-7] and chalchogenides,[39] consists of the stack of two-dimensional layers composed of edge-sharing SeH_4-tetrahedra network; within the layer both Se and H are four-fold coordinated. It is worth mentioning that in addition to this $P4/nmm$ phase, our structure search finds an energetically competitive $P2_1/c$ (Fig. 2d) structure (though metastable); it consists of complicated three-fold coordinated Se/H network. Turning to the H-rich H_3Se stoichiometry, the lowest-enthalpy structure has a high symmetry of Im-3m, similar to that of H_3S,[16] where Se atoms occupy a body-centered cubic sublattice, each Se being six-fold coordinated by H. This structure is transformed from a molecular $R3m$ phase as the result of pressure-induced hydrogen-bond symmetrization,[16] being stable above 166 GPa.

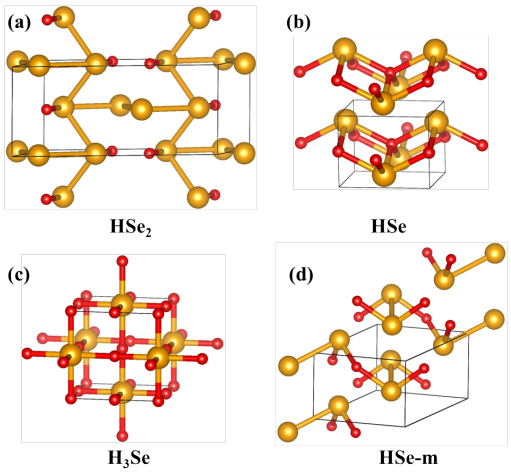

Figure 2. The energetically stable phases identified by the structure search: (a) HSe_2 in a $C2/m$ structure, (b) HSe in a $P4/nmm$ structure and (c) H_3Se in an Im-3m structure. For the HSe stoichiometry, the metastable $P2_1/c$ structure with competitive energetics (HSe-m) is also shown as (d). See Supplemental Table S1 for their detailed structural information.

Fig. 3a-c show the electronic band structure (with the projection onto H-s orbital) and projected density of states at 300 GPa for HSe_2, HSe and H_3Se, respectively. All the three phases exhibit metallic feature in their stable pressure region (see Supplemental Fig. S3). The conducting states around the Fermi level are predominated by the Se-p state, hybridizing in varying degrees with the H-s state in different phases. The H-rich H_3Se phase (Fig. 3c) shows the strongest hybridization, and the contribution of H-s state to the conducting states are remarkable and distributes in almost every band. For HSe (Fig. 3b), partial bands (*e.g.* along the A-M, M-Γ, X-Γ lines) are heavily derived from the H-s state. As to the Se-rich HSe_2 phase (Fig. 3a), only minority of bands crossing the Fermi level are moderately contributed by the H-s state. In H_3Se and HSe one can clearly see "flat band-steep band" feature in proximity to the Fermi level, potentially favoring strong electron−phonon coupling for good superconductivity.[41] Note that for all the phases there appear substantial amount of Se-d states around the Fermi level, due to the strong p-d

coupling at high pressures.[42] Analysis of the electron localization feature indicates a decreasing strength of covalent H-Se bond from H_3Se, HSe_2 to HSe (Supplemental Fig. S4), which is supported by their actual bond lengths [H_3Se (1.51 Å) < HSe_2 (1.57 Å) < HSe (1.69 Å) at 300 GPa].

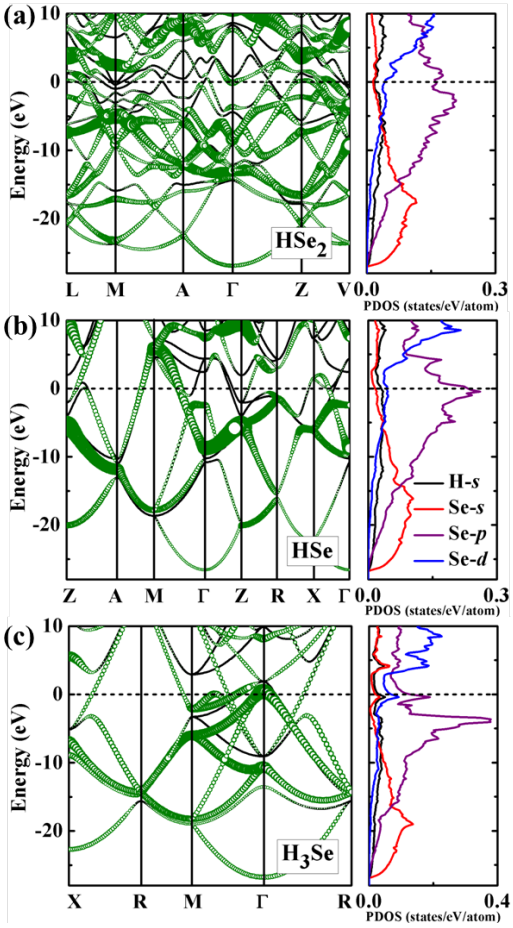

Figure 3. Electronic band structure (left panels) and projected density of states (right panels) at 300 GPa calculated at the DFT-PBE level for (a) HSe_2 in the *C*2/m structure, (b) HSe in the *P*4/nmm structure and (c) H_3Se in the *I*m-3m structure, respectively. The band structure has been projected onto the H-*s* orbital with the size of green circles proportional to the projection magnitude.

The phonon and electron-phonon coupling (EPC) calculations are performed for three predicted stable metallic species. The lattice dynamic stabilities of all the phases are clearly evidenced by the absence of any imaginary phonon mode in the whole Brillouin zone. The calculated phonon linewidth $\gamma_{q,j}(\omega)$, Eliashberg EPC spectral function $\alpha^2F(\omega)$ and EPC integration $\lambda(\omega)$ at 300 GPa are shown in Fig. 4. For H_3Se and HSe, the results of $\gamma_{q,j}(\omega)$ and $\alpha^2F(\omega)$ indicate that the most notable contribution to the EPC originate from high-frequency H-stretching modes. This is different from the cases in superconducting CaH_6[15] and SnH_4[17], where the medium-lying H-wagging vibrations contribute most significantly to the EPC. In view of the $\gamma_{q,j}(\omega)$ magnitudes along different q directions, the EPC is generally isotropic in HSe, but highly anisotropic in H_3Se. As for HSe_2, both high-lying H-stretching and moderate H-wagging modes show substantial contributions to the EPC, and the phonon linewidths maximize around the zone center. These analyses indicate that for all the three phases H atoms contribute significantly to the EPC. In particular, the specific contribution of H vibrations to the total EPC is 29.5%, 48.4% and 79.2% for HSe_2, HSe and H_3Se, respectively. The calculated total EPC parameter λ is 0.45 (HSe_2), 0.80 (HSe) and 1.04 (H_3Se). The latter two are comparable to the predicted values in H_2S,[20] falling in the range of fairly strong EPC. By using a typical value of the Coulomb

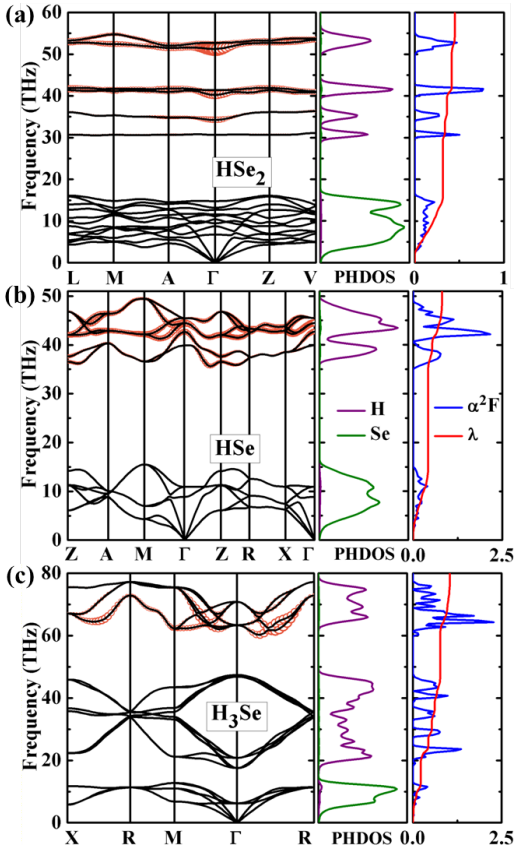

Figure 4. Phonon dispersion curves (left panels), phonon projected density of states (PHDOS, middle panels), Eliashberg electron–phonon coupling (EPC) spectral function $\alpha^2F(\omega)$ and EPC integration $\lambda(\omega)$ (right panels) at 300 GPa for (a) HSe_2 in the *C*2/m structure, (b) HSe in the *P*4/nmm structure and (c) H_3Se in the *I*m-3m structure, respectively. The phonon linewidth $\gamma_{q,j}(\omega)$ of each mode (*q*,*j*) caused by EPC is indicated (in left panels) by the orange circles, of which the sizes are proportional to linewidth magnitudes.

pseudopotential $\mu^* = 0.1$, together with the calculated logarithmic averaged phonon frequency ω_{log} (see Supplemental Table S2), we can estimate the superconducting critical temperature T_c via the Allen-Dynes modified McMillan equation. [43] The resulted values are 5 K, 42 K and 106 K for HSe_2, HSe and H_3Se, respectively.

After the completion of our work, we were aware of the work by Flores-Livas *et al*. (arXiv:1501.06336v1) predicting high temperature superconductivity (with the T_c up to 131 K) in selenium hydrides. Our work is different from theirs in several aspects: (i) They only focus on the H_3Se stoichiometry in analogy to H_3S, whereas we investigated the entire energy landscape of H-Se system by a more comprehensive global structure search. In addition to H_3Se, two more energetically stable stoichiometries (HSe_2 and HSe) are identified. (ii) We got a qualitatively different picture of energetic stability for selenium hydrides with respect to the elemental decomposition from theirs. Most of their structures are highly stable relative to the elemental decomposition, but in our work the energetically stable stoichiometries can only emerge at quite high pressures (above 100 GPa). (iii) In contrast to their work assuming H_3Se as the most stable stoichiometry, we find in fact H_3Se is marginally stable, and HSe_2 and HSe are the most stable species at medium and high pressure region, respectively. Our results underlie the synthesis of H_3Se in experiments may require particular kinetic control process.

To conclude, with the aim of finding stable and metallic selenium hydrides for potential high-T_c superconductors, we explore via a global minimum structure search method the hitherto unknown energy landscape of H-Se system at high pressures. Despite of similar electronic properties of S and Se, the high-pressure phase diagram of H-Se system is distinct from its H-S analogy. Three energetically stable phases, *i.e.* HSe_2, HSe and H_3Se, are identified. All of them exhibit metallic features and superconducting activities. The latter two are predicted to have a high T_c of 42 K (HSe) and 106 K (H_3Se). The HSe phase in the *P*4/nmm symmetry represents another interesting high-symmetry structure in addition to the intriguing *I*m-3m structure established in H_3S.[16] For such highly symmetric structures, the transition barriers between it and other isomers are usually high, which points to a strong kinetic stability with respect to variations of external conditions, thus favorable to experimental synthesis. Experimental attempt to synthesize these new phases and verification of their superconductivity are called for.

Acknowledgements. This research was supported by the China 973 Program (2011CB808200), Natural Science Foundation of China under Nos. 11274136, the 2012 Changjiang Scholars Program of China and the Postdoctoral Science Foundation of China under grant 2013M541283. L.Z. acknowledges funding support from the Recruitment Program of Global Experts (the Thousand Young Talents Plan).

REFERENCES

1. D. van Delft and P. Kes, Phys. Today. **63**, 38-43 (2010).
2. J. G. Bednorz and K. A. Müller, Zeitschrift für Physik B, **64**, 189-193 (1986).
3. G. F. Sun, K. W. Wong, B. R. Xu, Y. Xin and D. F. Lu, Phys. Lett. A. **192**, 122-124 (1994).
4. C. W. Chu, AAPPS Bulletin **18**, 9-21 (2008).
5. Y. Kamihara, H. Hiramatsu, M. Hirano, R. Kawamura, H. Yanagi, T. Kamiya and H. Hosono, J. Am. Chem. Soc. **128**, 10012-10013 (2006).
6. Y. Kamihara, T. Watanabe, M. Hirano and H. Hosono, J. Am. Chem. Soc. **130**, 3296-3297 (2008).
7. G. R. Stewart, Rev. Mod. Phys. **83** (4), 1589-1652 (2011).
8. M. L. Cohen, in BCS: 50 years (Ed Leon N. Cooper; Dmitri Feldman) 375-389 (2011).
9. L. Gao, Y. Y. Xue, F. Chen, Q. Xiong, R. L. Meng, D. Ramirez, C. W. Chu, J. H. Eggert and H. K. Mao, Phys. Rev. B **50**, 4260-4263 (1994).
10. Y. Bugoslavsky, Y. Miyoshi, G. K. Perkins, A. V. Berenov, Z. Lockman, J. L. MacManus-Driscoll, L. F. Cohen, A. D. Caplin, H. Y. Zhai, M. P. Paranthaman, H. M. Christen and M. Blamire, Supercond. Sci. Technol. **15**, 526-532 (2002).
11. N. W. Ashcroft, Phys. Rev. Lett. **21**, 1748-1749 (1968).
12. N. W. Ashcroft, Phys. Rev. Lett. **92**, 187002 (2004).
13. G. Gao, A. R. Oganov, A. Bergara, M. Martinez-Canales, T. Cui, T. Iitaka, Y. Ma and G. Zou, Phys. Rev. Lett. **101**, 107002 (2008).
14. Y. Li, G. Gao, Y. Xie, Y. Ma, T. Cui and G. Zou, Proc. Natl. Acad. Sci. U. S. A. **107**, 15708-15711 (2010).
15. H. Wang, J. S. Tse, K. Tanakab, T. Iitakac and Y. M. Ma, Proc. Natl. Acad. Sci. U. S. A. **109** (2011).
16. D. Duan, Y. Liu, F. Tian, D. Li, X. Huang, Z. Zhao, H. Yu, B. Liu, W. Tian and T. Cui, Scientific reports **4**, 6968 (2014).
17. G. Y. Gao, A. R. Oganov, P. Li, Z. Li, H. Wang, T. Cui, Y. Ma, A. Bergara, A. O. Lyakhov, T. Iitaka and G. Zou, Proc. Natl. Acad. Sci. U.S.A. **107**, 1317-1320 (2010).
18. R. Rousseau, M. Boero, M. Bernasconi, M. Parrinello and K. Terakura, Phys. Rev. Lett. **85**, 1254-1257 (2000).
19. M. Sakashita, H. Yamawaki, H. Fujihisa, K. Aoki, S. Sasaki and H. Shimizu, Phys. Rev. Lett. **79**, 1082-1085 (1997).
20. Y. W. Li, J. Hao, H. Liu, Y. Li and Y. M. Ma, J. Chem. Phys. **140**, 174712 (2014).
21. A. P. Drozdov, M. I. Eremets and I. A. Troyan, arXiv:1412.0460 (2014).
22. J. A. Flores-Livas, A. Sanna and E. K. U. Gross, arXiv:1501.06336 (2015).
23. D. A. Papaconstantopoulos, B. M. Klein, M. J. Mehl and W. E. Pickett, arXiv:1501.03950 (2015).
24. J. E. Hirsch and F. Marsiglio, arXiv:1412.6251 (2014).

25. A. P. Durajski, R. Szczesniak and Y. Li, arXiv:1412.8640 (2015).
26. J. H. Loehlin, P. G. Mennitt and J. S. Waugh, J. Chem. Phys. **44**, 3912 (1966).
27. Y. Wang, J. Lv, L. Zhu and Y. Ma, Phys. Rev. B, **82**, 094116 (2010).
28. Y. Wang, J. Lv, L. Zhu and Y. Ma, Comput. Phys. Commun. **183**, 2063-2070 (2012).
29. J. Lv, Y. Wang, L. Zhu and Y. Ma, Phys. Rev. Lett. **106**, 015503 (2011).
30. Y. Wang, H. Liu, J. Lv, L. Zhu, H. Wang and Y. Ma, Nat. Commun. **2**, 563 (2011).
31. L. Zhu, H. Liu, C. J. Pickard, G. Zou and Y. Ma, Nat. Chem. **6**, 645-649 (2014).
32. J. P. Perdew, J. A. Chevary, S. H. Vosko, K. A. Jackson, M. R. Pederson, D. J. Singh and C. Fiolhais, Phys. Rev. B, **46**, 6671-6687 (1992).
33. G. Kresse and J. Furthmuller, Phys. Rev. B, **54**, 11169-11186. (1996).
34. J. Kunes, R. Arita, P. Wissgott, A. Toschi, H. Ikeda and K. Held, Comp.Phys.Commun. **181**, 1888–1895 (2010).
35. P. Giannozzi, S. Baroni, N. Bonini, M. Calandra, R. Car, C. Cavazzoni, D. Ceresoli, G. L. Chiarotti, M. Cococcioni, I. Dabo, A. Dal Corso, S. de Gironcoli, S. Fabris, G. Fratesi, R. Gebauer, U. Gerstmann, C. Gougoussis, A. Kokalj, M. Lazzeri, L. Martin-Samos, N. Marzari, F. Mauri, R. Mazzarello, S. Paolini, A. Pasquarello, L. Paulatto, C. Sbraccia, S. Scandolo, G. Sclauzero, A. P. Seitsonen, A. Smogunov, P. Umari and R. M. Wentzcovitch, J. Phys. Condens. Matter. **21**, 395502 (2009).
36. P. Cherin and P. Unger, Inorg. Chem. **6**, 1589-1591 (1967).
37. M. I. McMahon, C. Hejny, J. S. Loveday, L. F. Lundegaard and M. Hanfland, Phys. Rev. B **70**, 054101 (2004).
38. C. J. Pickard and R. J. Needs, Nat. Phys. **3**, 473-476 (2007).
39. F. C. Hsu, J. Y. Luo, K. W. Yeh, T. K. Chen, T. Huang, P. M. Wu, Y. C. Lee, Y. L. Huang, Y. Y. Chu and D. C. Yan, Proc. Natl. Acad. Sci. U.S.A. **105**, 14262 (2008).
40. A. D. Becke and K. E. Edgecombe, J. Chem. Phys. **92**, 5397-5403 (1990).
41. A. Simon, Angew. Chem. Int. Ed. **36**, 1788-1806 (1997).
42. Y. M. Ma, M. Eremets, A. R. Oganov, Y. Xie, I. Trojan, S. Medvedev, A. O. Lyakhov, M. Valle and V. Prakapenka, Nature **458** (7235), 182-185 (2009).
43. P. B. Allen and R. C. Dynes, Phys. Rev. B **12**, 905-922 (1975).

Supplementary information

Phase Diagram and High-Temperature Superconductivity of Selenium Hydrides at High Pressures

Shoutao Zhang[1], Yanchao Wang[1], Hanyu Liu[1], Guochun Yang[2,*], Lijun Zhang[3,*] and Yanming Ma[1,*]

[1]*State Key Laboratory of Superhard Materials, Jilin University, Changchun 130012, China.*

[2]*Faculty of Chemistry, Northeast Normal University, Changchun 130024, China.*

[3]*College of Materials Science and Engineering, Jilin University, Changchun 130012, China*

[*]Address correspondence to: yanggc468@nenu.edu.cn, lijun_zhang@jlu.edu.cn or mym@calypso.cn

Index

page

Computational details

Our structural prediction approach is based on a global minimization of free energy surfaces merging *ab initio* total-energy calculations through CALYPSO (Crystal structure AnaLYsis by Particle Swarm Optimization) methodology as implemented in its same-name CALYPSO code.[1,2] The structures of stoichiometry H_nSe_m (n = 1 – 5 and m = 1 – 3) were searched with simulation cell sizes of 1−4 formula units (f.u.) at 0, 100, 200, and 300 GPa, respectively. In the first step, random structures with certain symmetry are constructed in which the atomic coordinates are generated by the crystallographic symmetry operations. Local optimizations using VASP code, [3] were done with the conjugate gradients method and were stopped when the enthalpy changes became smaller than 1×10^{-5} eV per cell. After processing the first generation structures, 60% of them with lower enthalpies are selected to produce the next generation structures by PSO. 40% of the structures in the new generation are randomly generated. A structure fingerprinting technique of bond characterization matrix is applied to the generated structures, so that identical structures are strictly forbidden. These procedures significantly enhance the diversity of the structures, which is crucial for the efficiency of the global search of structures. For most of the cases, the structure searching simulation for each calculation was stopped after we generated 1000 ~ 1200 structures (e.g., about 20 ~ 30 generations).

To further analyze the structures with higher accuracy, we select a number of structures with lower enthalpies and perform structural optimization using density functional theory within the generalized gradient approximation[4] as implemented in the VASP code. The cut-off energy for the expansion of wavefunctions into plane waves is set to 600 eV in all calculations, and the Monkhorst–Pack k-mesh with a maximum spacing of 0.03 $Å^{-1}$ was individually adjusted in reciprocal space with respect to the size of each computational cell. This usually gives total energy well converged within ~ 1 meV/atom. The electron-ion interaction was described by means of projector augmented wave with $1s^1$ and $3s^2 3p^4$ electrons as valence for H and Se atoms, respectively.

The relative stability of different H-Se compounds at each pressure is calculated using the following formula:

$$h_f(H_nSe_m) = [h(H_nSe_m) - nh(H) - mh(Se)]/(m+n) \quad (1)$$

where h_f is the enthalpy of formation per atom and h is the enthalpy for each compound.[5] Since H has a light atomic mass, its zero-point energy has an important contribution to the total energy. The effect of zero-point vibrational energy on stability of H-Se compounds is also included. The ZP vibrational energies are calculated by using the quasiharmonic model[6] as implemented in the phonopy code[7].

The electron-phonon coupling calculations are carried out by linear response density functional theory as implemented in the QUANTUM ESPRESSO package.[8] The norm-conserving pseudopotentials for H and Se are adopted. The kinetic energy cutoffs of 70 Ry are chosen for all phases. And 16 x 16 x 16 *k*-meshes and 4 x 4 x 4 q-meshes in the Brillouin zone are used for HSe_2 with *C*2/*m* structure, 18 x 18 x 24 k-meshes and 3 x 3 x 6 q-meshes in the Brillouin zone are used for HSe in a *P*4/*nmm* structure, 24 x 24 x 24 *k* meshes and 6 x 6 x 6 q meshes in the Brillouin zone are used for H_3Se in an *Im*-3*m* structure.

To further test the reliability of the adopted pseudopotentials for H and Se, other different pseudopotentials for H and Se are selected. Although there is little difference between them (Table S0), it shows that H_3Se indeed becomes stable above 150 GPa. LDA method also gives the same result. Moreover, the validity of the projector augmented wave (PAW) potentials from the VASP library is checked by comparing the calculated Birch-Murnaghan equation of state with that obtained from the full-potential linearized augmented plane-wave method using local orbitals (as implemented in WIEN2k).[9] The Birch-Murnaghan equation of states derived from VASP and WIEN2k methods are almost identical (Figure S0). Thus, our adopted pseudopotentials are feasible in the range of 0-300 GPa.

Table S0. Calculated formation enthalpy (eV) per formula unit of H_3Se with respect to H and Se using different pseudopotentials at 150 GPa.

PBE	**H**	**H_s**	**H_h**	**H_GW**
Se	-0.0092	-0.0193	-0.0105	-0.0105
Se_GW	-0.0079	-0.0180	-0.0093	-0.0093
LDA	**H**	**H_s**	**H_h**	**H_GW**
Se	-0.1531	-0.1538	-0.1536	-0.1538
Se_GW	-0.1528	-0.1534	-0.1533	-0.1534

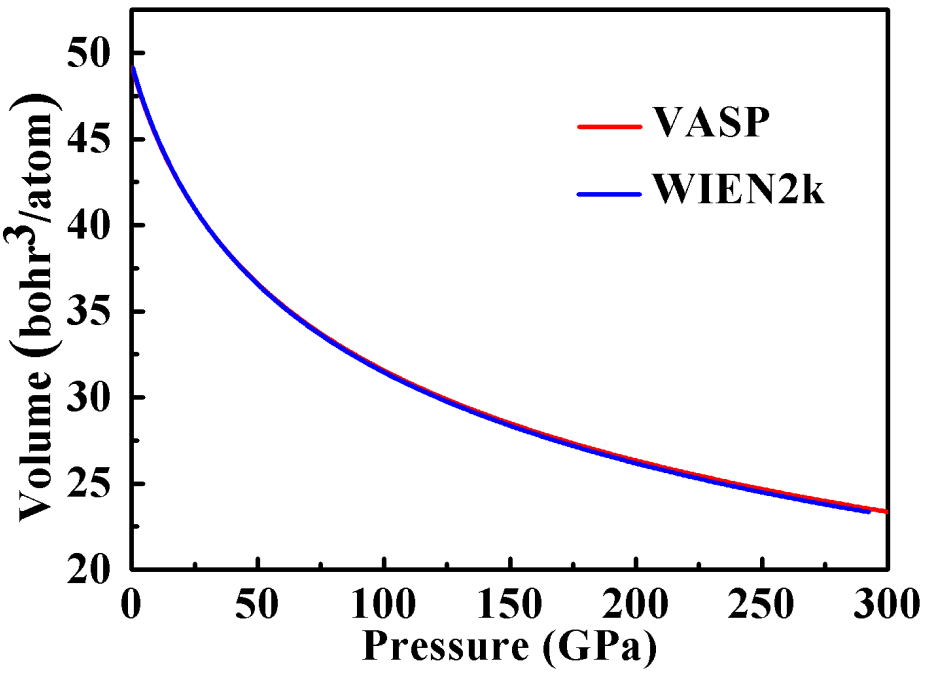

Figure S0. Comparing the Birch-Murnaghan equation of state by PAW and WIEN2K. The result indicates that the PAW potentials are applicable to H-Se compounds under high pressure.

Supplementary Figures

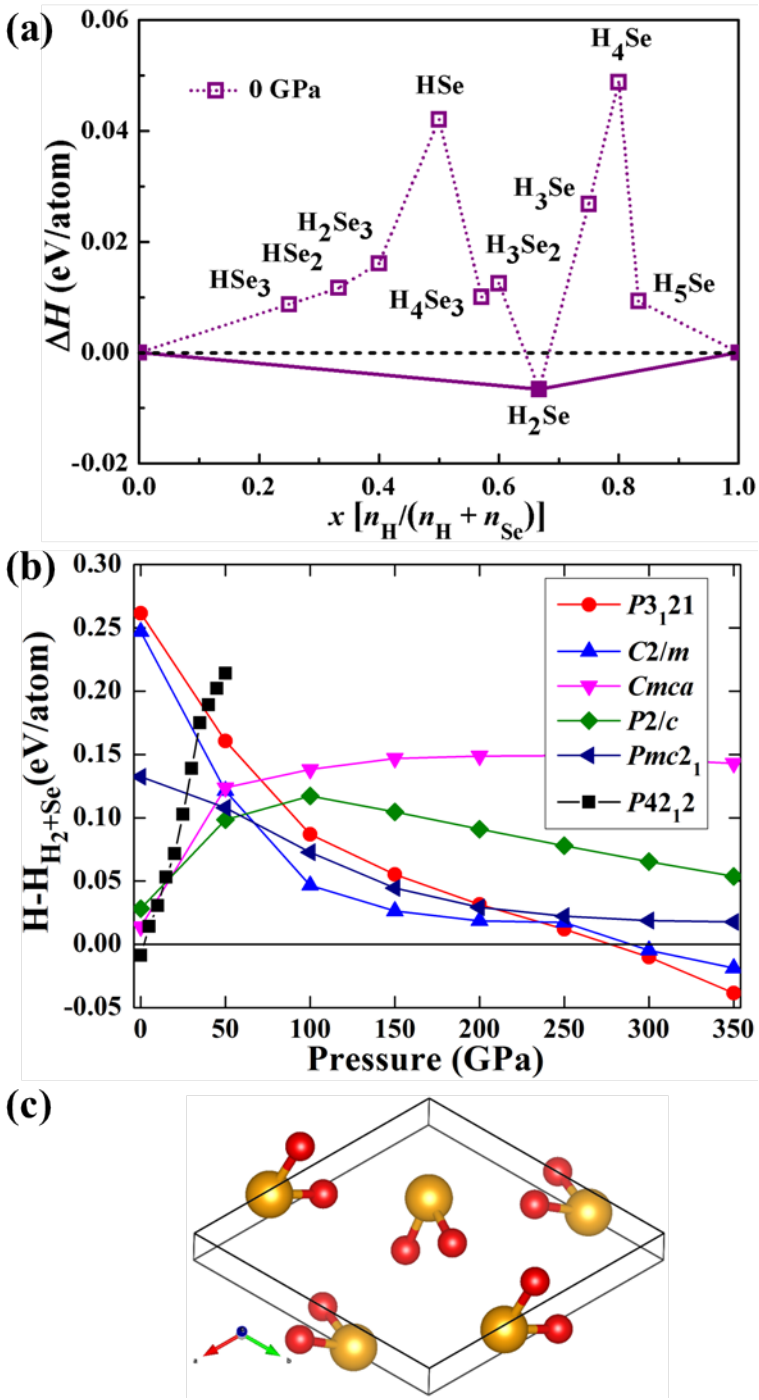

Figure S1. (a) Phase stabilities of H-Se compounds at pressures of 0 GPa. Predicted formation enthalpy of H-Se compounds with respect to decomposition into H_2 and selenium. Dashed lines0connect data points, and solid lines denote the convex hull. Compounds corresponding to data points located on the convex hull are stable against decomposition. (b) Calculated enthalpies per atom of various structures for

stoichiomety H_2Se in the pressure range of 0–350 GPa with respect to H_2+Se. (c) Predicted structure of H_2Se with $P3_121$ symmetry at 0 GPa.

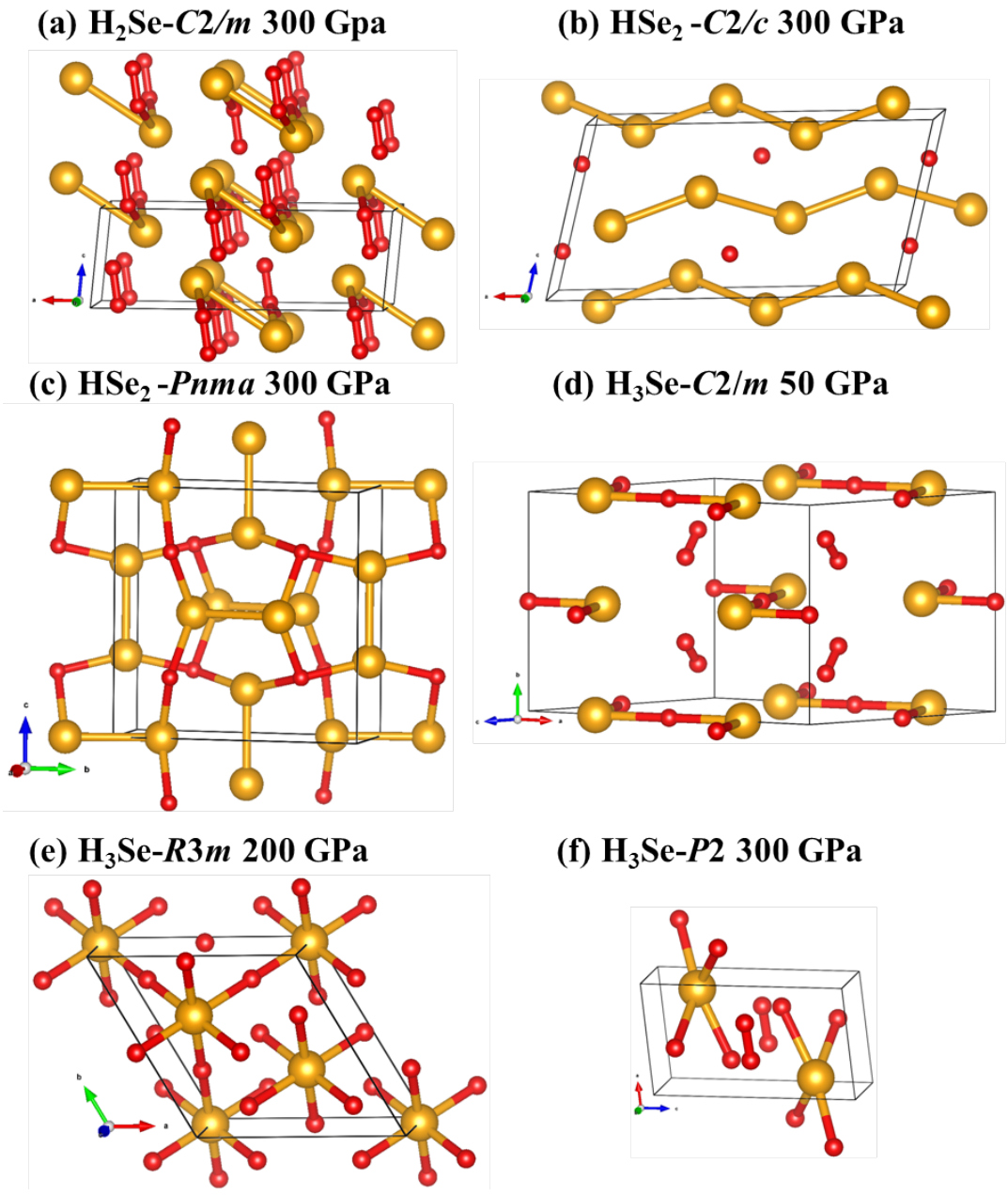

Figure S2. The metastable structures for stoichiometies H_2Se, HSe_2, and H_3Se.

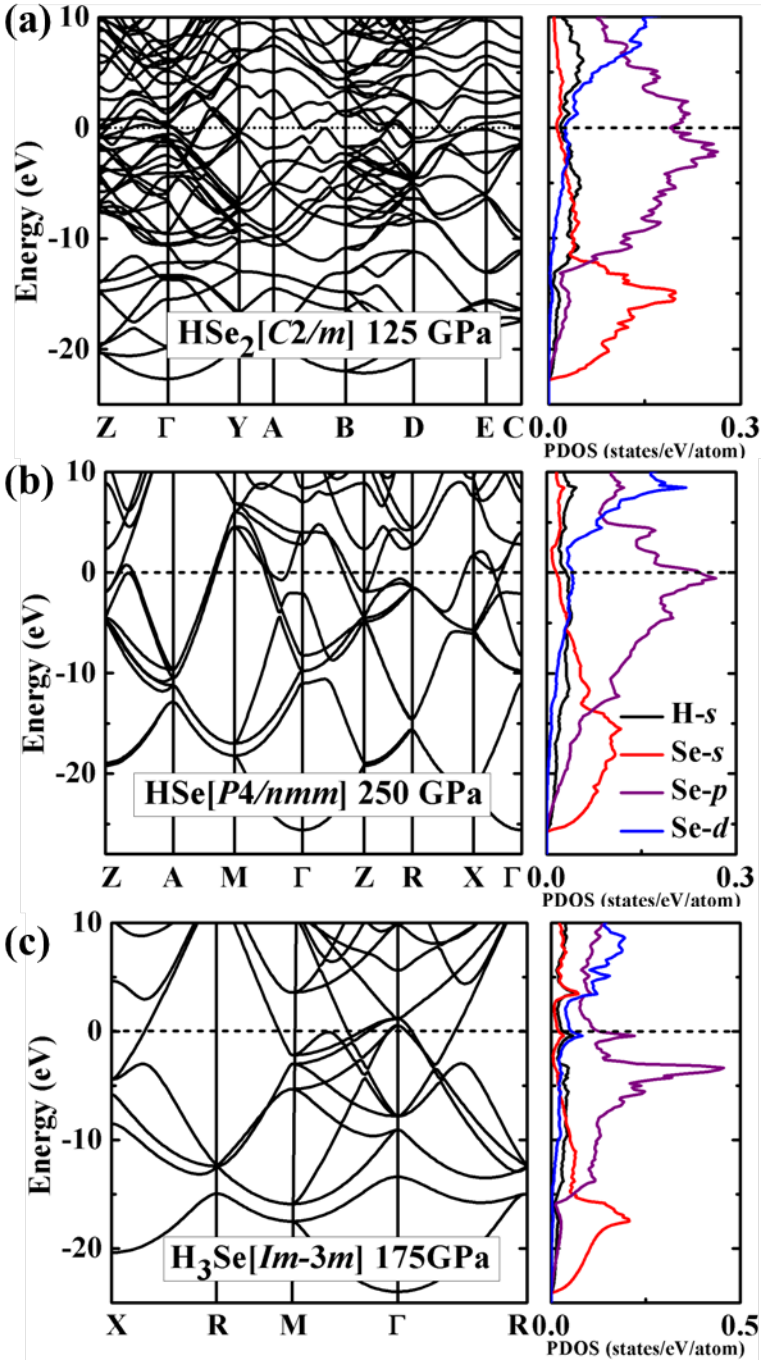

Figure S3. Electronic band structure (left panels) and projected density of states (right panels) calculated at the DFT-PBE level for (a) HSe_2[*C*2/*m*] at 125 GPa, (b) HSe[*P*4/*nmm*] at 250 GPa, and (c) H_3Se [*Im*-3*m*] at 175 GPa. The results show that the three compounds exhibit metallic at their stable pressure region.

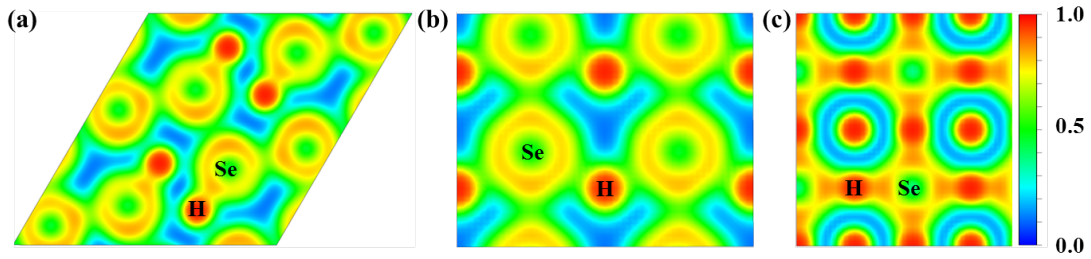

Figure S4. Electron localization function for HSe_2, HSe and H_3Se at 300 GPa

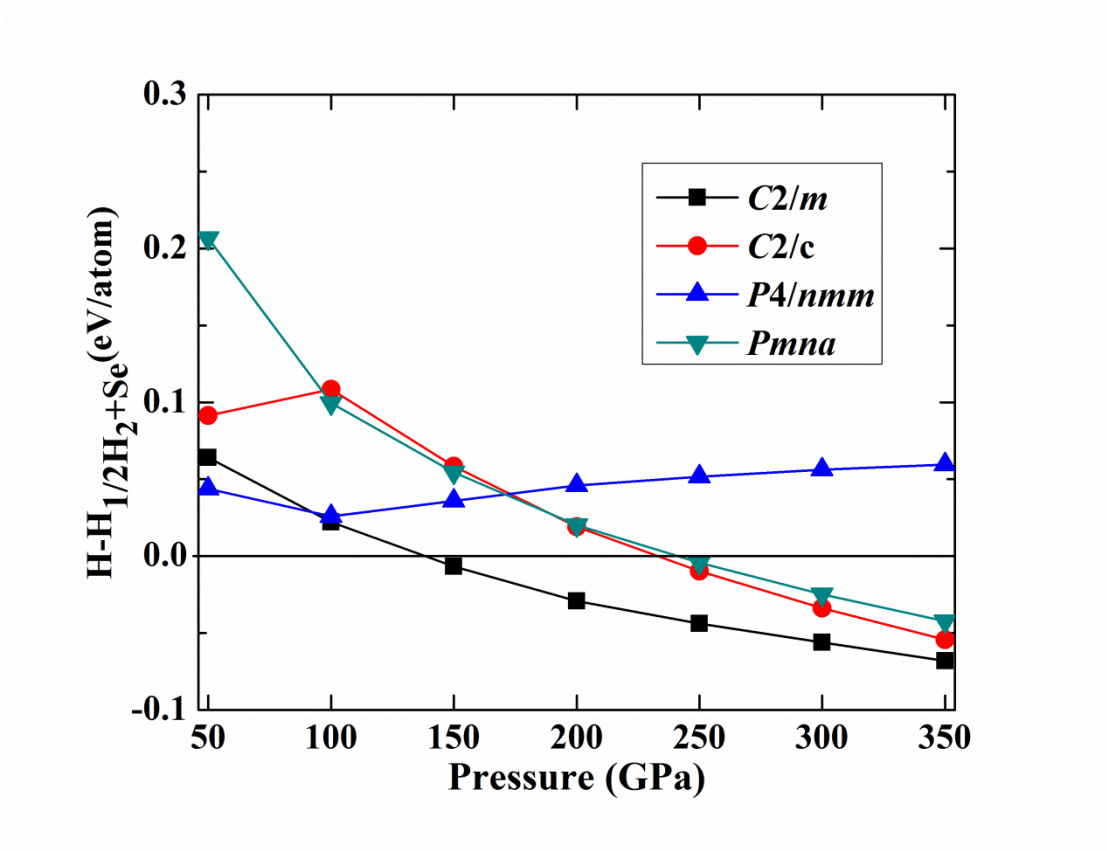

Figure S5. Calculated enthalpies of various structures per atom in the pressure range of 50–350 GPa with respect to $1/2H_2$+2Se.

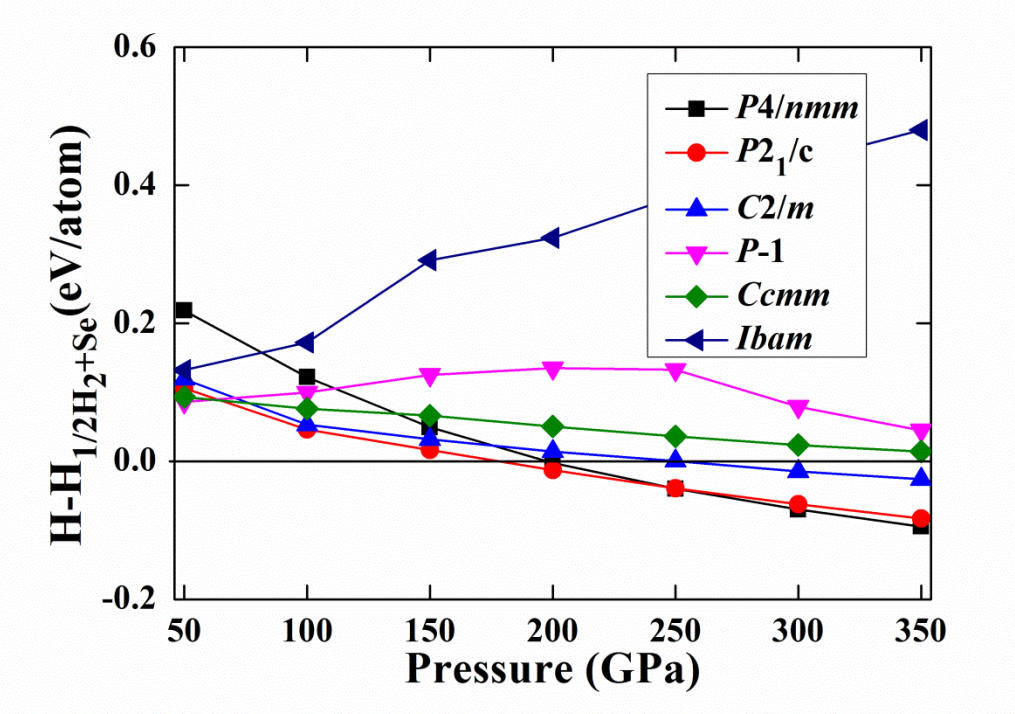

Figure S6. Calculated enthalpies per atom of various structures for stoichiometry HSe as functions of pressure between 0 and 350 GPa with respect to $1/2H_2$+Se.

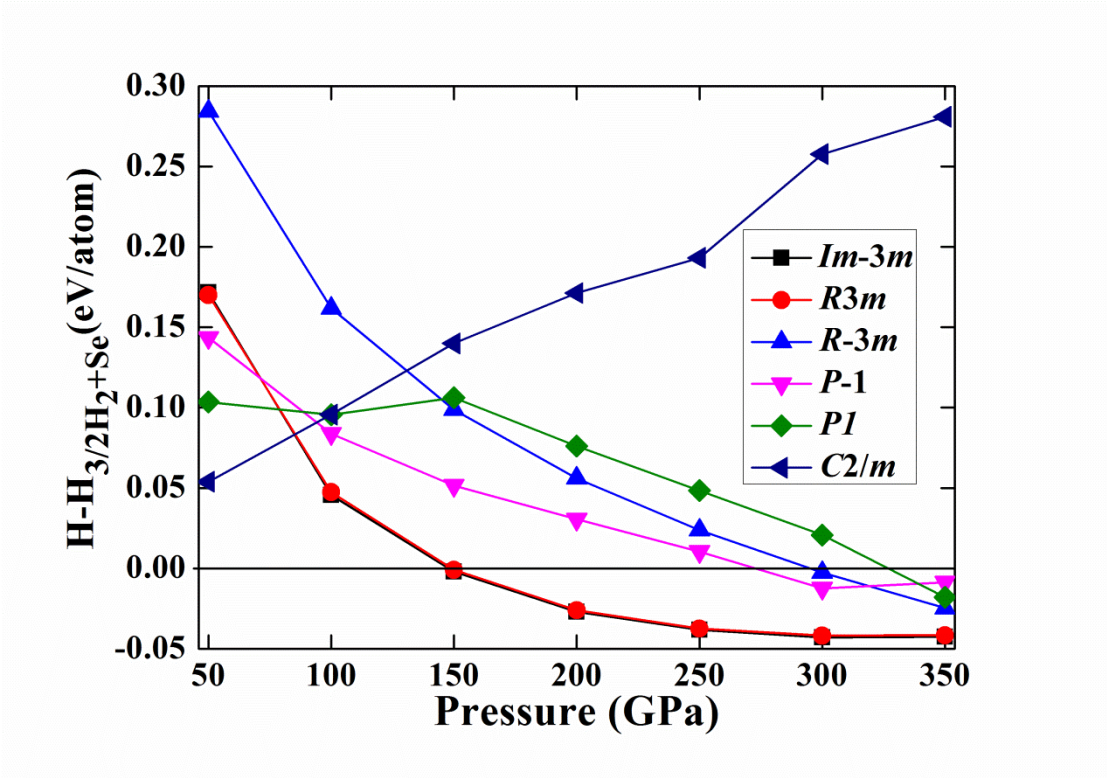

Figure S7. Calculated enthalpies per atom of various structures for stoichiometry H_3Se as functions of pressure between 50 and 350 GPa with respect to $3/2H_2$+Se.

Supplementary Tables

Table S1. Calculated structural parameters of the predicted stable structures for H-Se compounds at the selected pressure.

Phase	Pressure (GPa)	Lattice parameters (Å, °)	Atomic coordinates (fractional)			
HSe_2-*C2/m*	300	a = 7.580	H(4i)	0.376	0.000	0.288
		b = 3.222	Se(4i)	0.105	0.000	0.842
		c = 3.858	Se(4i)	0.355	0.000	0.672
		$\alpha = \gamma$ = 90.000				
		β = 120.320				
HSe-*P4/nmm*	300	$a = b$ =3.014	H(2b)	0.500	0.500	0.500
		c = 2.373	Se(2c)	0.500	0.000	0.817
		$\alpha = \beta = \gamma$= 90.000				
H_3Se-*Im-3m*	300	$a = b = c$ = 3.025	H(6b)	0.500	0.000	0.500
		$\alpha = \beta = \gamma$= 90.000	Se(2a)	0.500	0.500	0.500
HSe_2-*C2/m*	200	a = 7.897	H(4i)	0.376	0.000	0.288
		b = 3.310	Se(4i)	0.105	0.000	0.842
		c = 4.048	Se(4i)	0.355	0.000	0.672
		$\alpha = \gamma$ =90.000				
		β = 120.341				
H_3Se-*Im-3m*	200	$a = b = c$ = 3.148	H(6b)	0.500	0.000	0.500
		$\alpha = \beta = \gamma$= 90.000	Se(2a)	0.500	0.500	0.500
H_2Se-$P3_121$	0	$a = b$ =5.873	H(6c)	0.900	0.450	0.030
		c = 6.871	Se(3b)	1.320	0.320	0.500
		$\alpha = \beta$ = 90.000				
		γ =120.000				

Table S2. Calculated critical temperatures (*T*c) of the three stable compounds at 300 GPa. (HSe_2 with *C*2/*m* structure, HSe in a *P*4/*nmm* structure, and H_3Se in an *Im*-3*m* structure.) Lambda is the electron phonon coupling parameter; Omega_log (K) is the logarithmic average of the α^2F function; T_c is the critical temperature.

300 GPa	**lambda**	**omega_log (K)**	T_c**(K)**
HSe_2	0.44827	646.780	4.903
HSe	0.80443	885.005	41.941
H3Se	1.04235	1436.014	106.417

Reference

(1) Wang, Y.; Lv, J.; Zhu, L.; Ma, Y. Crystal Structure Prediction via Particle-Swarm Optimization. *Phys. Rev. B* **2010**, *82*, 094116.

(2) Wang, Y.; Lv, J.; Zhu, L.; Ma, Y. CALYPSO: A Method for Crystal Structure Prediction. *Comput. Phys. Commun*. **2012**, *183*, 2063.

(3) Kresse, G.; Furthmuller, J. Efficient Iterative Schemes for ab initio Total-Energy Calculations Using a Plane-Wave Basis Set. *Phys. Rev. B* **1996**, *54*, 11169.

(4) Perdew, J. P.; Chevary, J. A.; Vosko, S. H.; Jackson, K. A.; Pederson, M. R.; Singh, D. J.; Fiolhais, C. Atoms, Molecules, Solids, and Surfaces: Applications of the Generalized Gradient Gpproximation for Exchange and Correlation. *Phys. Rev. B* **1992**, *46*, 6671.

(5) Feng, J.; Hennig, R. G.; Ashcroft, N. W. & Hoffmann, R. Emergent reduction of electronic state dimensionality in dense ordered Li–Be alloys. *Nature*, **2008**, *451*, 445.

(6) Dove, M. T. Introduction to lattice dynamics, Cambridge university press. **1993**, ISBN 0521392934.

(7) Togo, A.; Oba, F. & Tanaka, I. First-principles calculations of the ferroelastic transition between rutile-type and $CaCl_2$-type SiO_2 at high pressures. *Phys. Rev. B* ***2008****, 78,* 134106.

(8) Giannozzi, P.; Baroni, S.; Bonini, N.; Calandra, M.; Car, R.; Cavazzoni, C.; Ceresoli, D.; Chiarotti, G.; Cococcioni, M.; Dabo, I.; Corso, A.; de Gironcoli, S.; Fabris, S.; Fratesi, G.; Gebauer, R.; Gerstmann, U.; Gougoussis, C.; Kokalj, A.; Lazzeri, M.; Martin-Samos, L.; Marzari, N.; Mauri, F.; Mazzarello, R.; Paolini, S.; Pasquarello, A.; Paulatto, L.; Sbraccia, C.; Scandolo, S.; Sclauzero, G.; Seitsonen, A.; Smogunov, A.; Umari, P.; Wentzcovitch, R. QUANTUM ESPRESSO: a Modular and Open-source Software Project for Quantum Simulations of Materials. *J. Phys.: Condens. Matter.* **2009**, *21*, 395502.

(9) Kunes, J.; Arita, R.; Wissgott, P.; Toschi, A.; Ikeda H.; Held, K. *Comp. Phys. Commun.* **2010**, *181*, 1888–1895.